Flow-enhanced nucleation of poly(1-butene) : model application to short-term and continuous shear and extensional flow

Flow-enhanced nucleation of poly(1-butene): Model application to short-term and continuous shear and extensional flow

Peter C. Roozemond and Gerrit W. M. Peters[a)]

Department of Mechanical Engineering, Eindhoven University of Technology, P.O. Box 513, 5600MB Eindhoven, The Netherlands

(Received 13 January 2013; final revision received 4 July 2013; published 25 September 2013)

Synopsis

A modeling framework for flow-enhanced nucleation of polymers is applied to a broad set of data from literature. Creation of flow-induced pointlike nuclei is coupled to chain stretch of the high-molecular weight tail of the material, calculated with a rheological constitutive model. As the flow-induced nuclei grow, the crystalline volume fraction increases and with it the viscosity of the material. This is accounted for by describing the material as a suspension of spheres in a viscoelastic matrix. Calculations are compared with a broad set of experimental data from literature on three grades of poly(1-butene). First, a parameter set is determined by fitting model results to flow-induced nucleation densities from short-term shear experiments. Next, this parameter set is used to validate the framework in continuous flow experiments in which viscosity is monitored during a constant flow rate. In this way, we demonstrate the approach is applicable to not only short-term shear but also continuous flow. It was observed in experiments that for continuous extensional flow, the viscosity shows an upturn at a constant strain, the value of which is independent of strain rate. We hypothesize that this upturn is related to long chains entering the chain stretch regime, as a result of the extension rate exceeding the inverse of the Rouse time of the longest chains. © *2013 The Society of Rheology*. [http://dx.doi.org/10.1122/1.4821609]

I. INTRODUCTION

The mechanical and optical properties of semicrystalline polymer products strongly depend on crystalline structure [Meijer and Govaert (2005); Schrauwen *et al*. (2004a, 2004b); van Erp *et al*. (2009)], which is largely determined by processing conditions [Janeschitz-Kriegl *et al*. (2003); van Meerveld *et al*. (2004)]. The development of a predictive model for flow-induced crystalline structure formation is therefore a vital step toward predicting properties of polymer products.

The majority of experimental work on flow-induced crystallization (FIC) has followed the short-term shear protocol proposed by the group of Janeschitz-Kriegl [Liedauer *et al*. (1993)]; it was spawned by the idea that if the crystallization time is much longer than flow time, it can be assumed that the only effect of flow is creation of structure; crystalline growth rate is unaffected. Because of the short flow times, this method is suitable for

[a)]Author to whom correspondence should be addressed; electronic mail: g.w.m.peters@tue.nl

investigating FIC up to flow rates that are relevant for industrial processing conditions. Important findings include the dominant role of the high-molecular weight (hmw) tail in creating nucleation sites [Balzano *et al.* (2008); Kimata *et al.* (2007); Mykhaylyk *et al.* (2008); Seki *et al.* (2002); Vleeshouwers and Meijer (1996)] and the importance of various rheological timescales in the material [van Meerveld *et al.* (2004)].

Alternatively, FIC can be investigated in a continuous flow experiment. In these types of experiments, the material is subjected to a constant flow rate in a rheometer, and the viscosity is monitored. At a certain point in time, the viscosity will show an upturn due to crystallization. The time at which this happens is a measure for the crystallization-enhancing effect of flow. These types of experiments have been performed in rotational flow [Acierno *et al.* (2008); Hadinata *et al.* (2005)] as well as extensional flow [Derakhshandeh and Hatzikiriakos (2012); Hadinata *et al.* (2007); White *et al.* (2012)]. Flow times are typically higher than for short-term flow experiments, which at high-shear rates might result in destruction of the sample. Therefore, this approach is mainly suited for low shear or extension rates.

The derivation of a predictive model for FIC has been attempted in a number of ways. Some researchers started with the classical result for homogeneous nucleation known as the Hoffman/Lauritzen expression [Acierno *et al.* (2008); Coppola and Grizzuti (2001)], which contains the free energy as a driving force. The entropic part is adapted by including the decrease due to the molecular orientation caused by the flow. A model using this approach was derived by Ziabicki and Alfonso (2002), but the entropy change due to orientation alone could not reproduce effects as dramatic as observed in experiments. A second approach starts from the statistical description of the evolution of the precursor size distribution in the melt [Ziabicki and Alfonso (1994)] and, again, incorporates the effect of flow by adapting the free energy. On the level of the precursors, a Monte-Carlo approach was used by Graham and Olmsted (2009, 2010), leading to insight into the relation between segmental orientation and the nucleation process and providing support for modeling on a continuum level, although this approach is not useful on the level of process modeling due to computational expensiveness. Based on experimental observations, Eder and Janeschitz-Kriegl (1997) proposed a set of differential equations analogous to the Schneider rate equations [Schneider *et al.* (1988)] for point nucleation and subsequent spherulitical growth that captured the observed correlations between measures for crystalline structure (i.e., number and size of fibrils) and the applied flow. Shear rate was used as the driving force for flow-enhanced nucleation and subsequent fibrillar growth.

Taking this set of equations, Zuidema *et al.* (2001) replaced the shear rate with the second invariant of the deviatoric part of the stress in the hmw tail, a measure that combines the molecular orientation and stretch. This phenomenological approach successfully captured the vast amount of experimental observations on isotactic polypropylene (iPP) from the group of Eder and Janeschitz-Kriegl. The nucleation model was studied and validated further by Custodio *et al.* (2009) and Steenbakkers and Peters (2011). Applied to iPP, the model captures short-term shear experimental results very well, in simple shear [Roozemond *et al.* (2011); Steenbakkers and Peters (2011); van Erp (2012)] as well as in channel flow [Custodio *et al.* (2009); Zuidema *et al.* (2001)]. Steenbakkers (2009) applied the model to data on poly(1-butene) from the group in Leuven, who studied this material extensively [Baert and van Puyvelde (2006); Baert *et al.* (2006)]. Roozemond *et al.* (2011) showed that a similar model derived from the concept of flow-activatable dormant precursors [Janeschitz-Kriegl and Ratajski (2005); Janeschitz-Kriegl *et al.* (2003)] yields qualitatively comparable results.

In this work, we study the predictive capability in continuous flow of the nucleation model first developed by Zuidema. To this end, we compare calculations with experimental

data from various sources on three grades of isotactic poly(1-butene) (iP1B) of which the rheology was well-characterized. Parameters for the nucleation model are first determined from fitting to short-term shear experiments [Ottonello (2003)]. Then, using the same parameters, the model is validated in continuous simple shear and uniaxial extension flow [Acierno *et al.* (2008); Hadinata *et al.* (2007, 2005)]. The Schneider rate equations [Schneider *et al.* (1988)] and a suspension model [Roozemond *et al.* (2012); Steenbakkers and Peters (2008)] are used to calculate crystalline volume fraction and resulting viscosity increase in time. The goal of this paper is not to improve or adapt the existing model but rather to investigate how well the experimental data presented here could be captured by the model and, if required, could be used for model improvement in future work.

In Sec. II, we give some material characteristics and information about the experiments. The modeling framework is presented in Sec. III. Experimental results and calculations are compared in Sec. IV. The conclusions from this work are summarized in Sec. V.

II. EXPERIMENTAL

A. Materials

Three commercial grades of iP1B, produced by LyondellBasell, were used in the experiments to which calculations are compared in this study. Information about the molecular weight distributions are given in Table I. A multimode Maxwell spectrum was fitted to rheological data from literature, see Fig. 1 and Table II. The reptation time of the slowest Maxwell mode, corresponding to the inverse of the oscillatory frequency at the onset of the terminal regime, was taken as the relaxation time representing the hmw tail for our nucleation model. The corresponding Rouse time was calculated using [Doi and Edwards (1986)]

$$\lambda_{\mathrm{R}} = \frac{\lambda_{\mathrm{rep}}}{3Z}, \tag{1}$$

where Z is the number of entanglements per chain as in Table I. The molecular weight between entanglements was taken as $M_e = 18\,\mathrm{kg/mol}$ [Baert *et al.* (2006)]. The Rouse times of the longest modes, which are used to calculated stretch for input in the nucleation model, are given for all materials at 100 °C in Table III.

It is well known that P1B can crystallize in a number of polymorphs [cf. Danusso (1967)]. Crystals from the melt form in the kinetically favorable phase II, which after solidification transform to the stable phase I. This transformation is relatively slow and does not take place during the experiments with conditions as discussed here [Baert *et al.* (2006)].

TABLE I. Molecular and rheological properties (M_n is number average molecular weight, M_w is weight average molecular weight, M_e is molecular weight between entanglements, E_a is flow activation energy, T_m^0 is thermodynamic melting point) [Azzurri (2003); Baert and van Puyvelde (2006); Hadinata (2007); Hadinata *et al.* (2005)].

	PB800	PB400	BR200
M_w (kg/mol)	85	176	762
M_w/M_n	5.1	5.7	19.6
$Z = M_w/M_e$	4.7	9.8	42
Isotacticity (*mmmm*)	79.5	79.5	89.9
E_a (kJ/mol)	41.0	47.2	54.7
T_m^0 (°C)	130.4	134.0	138.1

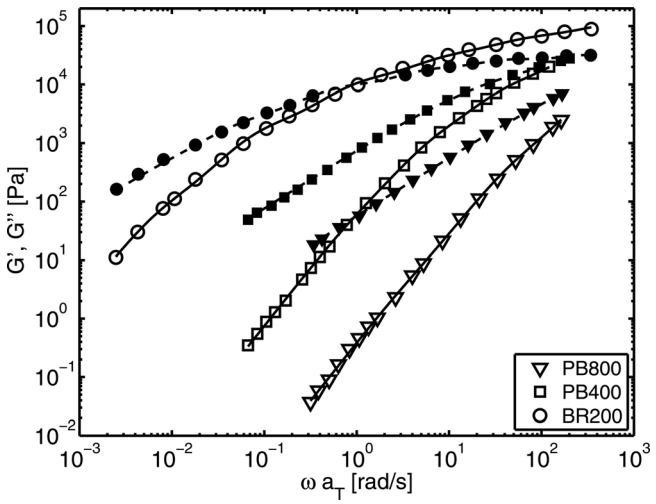

FIG. 1. Storage and loss moduli of the three grades at a reference temperature of 180 °C. Open symbols show measured storage modulus, closed symbols show measured loss modulus. Solid and dashed lines give storage and loss moduli from the Maxwell spectrums given in Table II. Data for PB800 and PB400 from Baert (2009), data for BR200 from Hadinata *et al*. (2005).

All crystallites in these conditions form in phase II and the transformation to form I is outside the scope of this work.

To calculate space filling during continuous shear using the Schneider rate equations, the crystal growth rate is used. Data for all three grades are shown in Fig. 2.

B. Short-term shear flow experiments

Short-term shear experiments were performed at the University of Genova on grades PB800 and BR200 in a Linkam CSS 450 rotational shearing device [G. Alfonso (personal communication); Ottonello (2003)]. Thermomechanical history was erased at 180 °C before cooling down to a temperature where a shear pulse was applied. The shear rate, shear time, and shear temperature were varied. For PB800, the shear temperature T_{shear} was varied between 83 and 97 °C; for BR200 $T_{\text{shear}} \in (100, 160)$ °C. After shear, the material was monitored using optical microscopy. The number of nuclei in the observation window was counted from which nucleation density was estimated. PB800 was held at the shear temperature to crystallize; the BR200 samples were cooled down to 92 °C because of the low growth rate at the shear temperatures. These experimental results were used to determine the parameters in the nucleation model.

TABLE II. Relaxation times and moduli of Maxwell spectra at 180 °C.

PB800		PB400		BR200	
λ_k (s)	$G_k \cdot 10^3$ (Pa)	λ_k (s)	$G_k \cdot 10^3$ (Pa)	λ_k (s)	$G_k \cdot 10^3$ (Pa)
0.0018	25.5	0.0036	52.9	0.0027	54.6
0.018	0.64	0.029	10.6	0.024	34.3
0.25	0.0020	0.15	1.53	0.16	22.1
		0.89	0.040	1.4	11.4
				13.7	2.2
				125	0.10

TABLE III. Rouse times of the hmw tail of the materials at 100 °C.

	PB800	PB400	BR200
$\lambda_{R,hmw}$ (s)	0.18	0.44	22.5

C. Continuous flow experiments

Calculations are compared with results from continuous flow experiments from various sources [Acierno *et al*. (2008); Hadinata *et al*. (2007, 2005)]. In these types of experiments, the polymer melt is subjected to a constant shear or extension rate in a rheometer while the viscosity is monitored. For shear, a plate-plate setup is used. Uniaxial extensional flow experiments were done using an extensional viscosity fixture (EVF), which was introduced by Sentmanat (2004). We will compare predictions from the model and experimental data for the transient viscosity signal for rotational and extensional rheometries. Hadinata *et al*. (2005) showed, using *ex-situ* optical microscopy, that for the shear experiments, all crystallites were isotropic spherulites. Therefore, the assumption that only isotropic structures are formed holds for the shear experiments. The experiments with extensional flow, which are described in Sec. IV, might yield oriented structures.

III. THEORY

A. Nucleation model

The aim of the present work is to demonstrate the applicability of this approach to short-term shear as well as continuous flow. To this end, the full model formulation as first developed by Zuidema *et al*. (2001) and improved by Steenbakkers and Peters (2011) was simplified in some aspects. In the range of flow conditions of interest in this work, the effect of these simplifications is minor while considerably reducing the number of fitting parameters. In this section, we present only the governing equations of the simplified model, the simplifications with respect to the full model are discussed in Appendix A.

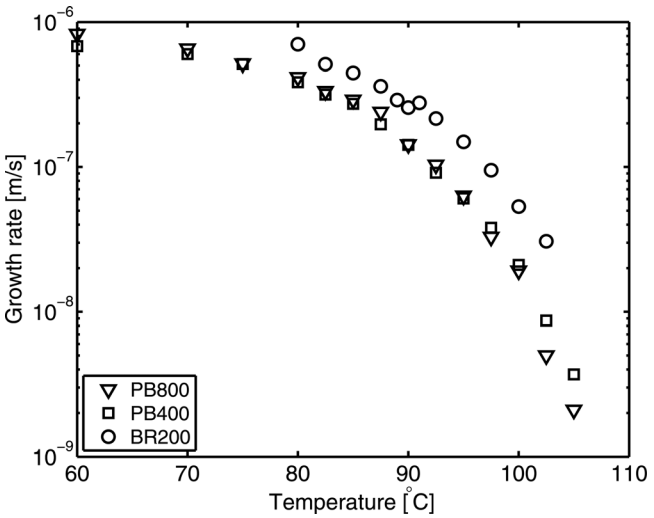

FIG. 2. Crystal growth rate of the three grades as a function of temperature from Azzurri (2003).

The polymer chains orient and stretch as the material is subjected to deformation. Regions with highly stretched molecules can act as nucleation sites. In a polydisperse melt, this effect is most pronounced for the hmw chains of the material, as these are more susceptible to deformation than shorter chains. The creation rate of flow-induced nuclei is coupled to the stretch in the hmw tail of the material. This is expressed as

$$\frac{dN_{nf}}{dt} = g_n\left(\Lambda_{\mathrm{hmw}}^4(t) - 1\right). \tag{2}$$

Here, N_{nf} is the number density of flow-induced nuclei and g_n is a scaling parameter which depends on temperature and pressure [van Erp (2012)], and presumably also the chemical properties of the material, such as isotacticity and the presence of nucleating agents. Λ_{hmw} is the average stretch of the long chains in the material, whose evolution during flow can be calculated using a continuum-level rheological model such as the Phan-Thien Tanner [Phan-Thien (1978); Phan-Thien and Tanner (1977)], Rolie-Poly [Likhtman and Graham (2003)], or eXtended Pom-Pom model [Verbeeten *et al.* (2004)] if the relevant parameters (e.g., relaxation times) are known. Steenbakkers and Peters (2011) tested several functions of Λ_{hmw} and found the fourth power to give closest agreement with experimental results. In this study, we take the slowest mode of a multimode Maxwell spectrum (Table II) as representative for the hmw tail. The Rolie-Poly model is used to calculate the stretch of the chains in the flow field. The extra stress is given by

$$\boldsymbol{\sigma} = \sum_i G(\boldsymbol{B}_{e,i} - \boldsymbol{I}), \tag{3}$$

with $\boldsymbol{B}_{e,i}$ the elastic Finger tensor of mode i obtained from the Rolie-Poly differential constitutive equation as given by Likhtman and Graham (2003)

$$\frac{d\boldsymbol{B}_{e,i}}{dt} = \boldsymbol{L}\cdot\boldsymbol{B}_{e,i} + \boldsymbol{B}_{e,i}\cdot\boldsymbol{L}^T - \frac{1}{\lambda_{\mathrm{rep},i}}(\boldsymbol{B}_{e,i} - \boldsymbol{I}) - \frac{1}{\lambda_{R,i}}\left(1 - \frac{1}{\Lambda_i}\right)\left(\boldsymbol{B}_{e,i} + \beta\Lambda_i^{2\delta}(\boldsymbol{B}_{e,i} - \boldsymbol{I})\right), \tag{4}$$

with $\boldsymbol{L} = \nabla v$ the rate of deformation tensor, and the stretch parameter

$$\Lambda_i = \sqrt{\frac{\mathrm{tr}(\boldsymbol{B}_{e,i})}{3}}. \tag{5}$$

Likhtman and Graham (2003) found the best agreement with experimental data if convective constraint release was turned off; $\beta = 0$ in Eq. (4). Steenbakkers and Peters (2011) found that this also gave the most accurate results in the nucleation model. Therefore, we take $\beta = 0$.

B. Self-enhancing effect

Ordering events are most likely to occur at the molecules in the hmw tail, as these are more susceptible to be stretched than shorter chains. The ordered structures limit the mobility of these hmw chains, thereby acting as additional entanglements on these chains. Effectively, these cause the relaxation times of the hmw tail of the material to increase with the number of flow-induced nuclei. A self-reinforcing effect is the result: If the material contains a large amount of flow-induced nuclei, it will have increased relaxation times and hence be more susceptible to further flow-enhanced nucleation. This mechanism is captured straightforwardly by

$$\frac{\lambda_{j,\mathrm{hmw}}}{\lambda_{j,\mathrm{hmw},0}} = (1 + \alpha N_{nf}), \tag{6}$$

with $j \in \{\mathrm{rep}, \mathrm{R}\}$, the reptation and Rouse time, respectively. α is a scaling parameter.

Zuidema *et al.* (2001) introduced the above as a necessary addition to the core of the model, which is the coupling between chain stretch and nucleation. Although such a phenomenon would be very hard to measure experimentally, there are clear indications for changes in the rheology of a crystallizing melt during the early stages of crystallization, even when the spherulites are still too small to have a noticeable effect on the viscosity, if the behavior of the material is purely suspension-like [Bove and Nobile (2002); Carrot *et al.* (1993); Roozemond *et al.* (2012)]. It is obvious that the nuclei do not create the junction points in a percolating network because they are too far apart (with radius of gyration of chains $R_g = 10$–$100\,\mathrm{nm}$ and distance between spherulites 10–100 μm), but the mechanism for slowing down of chains involved in nuclei can be of a different nature. For example, one could think of a mechanism of "incubators": Local regions around a nucleus where mobility is decreased, where the probability of further nucleation is increased [Steenbakkers (2009)].

Additionally, not all structures that are created by flow actually crystallize. There is ample evidence of structures (usually referred to as "precursors") forming that do have a certain kind of order [Azzurri and Alfonso (2005, 2008); Janeschitz-Kriegl *et al.* (2003); Ma *et al.* (2012)] but that are not crystalline/that do not grow into spherulites. These structures might also have an effect of the mobility of chains.

Because of the lack of direct evidence, the exact mechanism remains indiscernible. Therefore, we use the most straightforward way of representing this effect, in the form of Eq. (6). We should note that in the results of this paper, this effect, although important, is minor. α is in the order of $10^{-14}\,\mathrm{m}^3$ and N_{nf} is maximum $10^{14}\,\mathrm{m}^{-3}$, hence the relaxation time is increased by at most a factor of two. In simulations with stronger flow conditions [Custodio *et al.* (2009); Steenbakkers and Peters (2011); Zuidema *et al.* (2001)], the effect is more pronounced. Finally, as we show in Sec. V B 2, this effect cannot be observed in the viscosity in continuous flow.

IV. CONTINUOUS FLOW

The viscosity increase in our calculations of continuous flow is caused by a combination of two effects. First, the reptation and Rouse time of the hmw tail increases as described above. Second, the material can be viewed as a suspension of soft particles (the growing spherulites) in a viscoelastic matrix (the amorphous melt) [Roozemond *et al.* (2012); Steenbakkers and Peters (2008)]. As the spherulites grow, the viscosity of the material increases. For low shear rates, where the nucleation density is close to that of a quiescent melt, the viscosity increase is solely caused by the latter phenomenon. The undisturbed volume fraction of the crystalline phase was modeled using the Schneider rate equations [Schneider *et al.* (1988)], which for isothermal conditions and a fixed nucleation density reduces to the well-known Avrami analysis,

$$\begin{aligned}
\dot{\phi}_3 &= 8\pi\dot{N} \qquad (\phi_3 = 8\pi N),\\
\dot{\phi}_2 &= G\phi_3 \qquad (\phi_2 = 8\pi R_{\mathrm{tot}}),\\
\dot{\phi}_1 &= G\phi_2 \qquad (\phi_1 = S_{\mathrm{tot}}),\\
\dot{\phi}_0 &= G\phi_1 \qquad (\phi_0 = V_{\mathrm{tot}}),
\end{aligned} \tag{7}$$

where $\dot{N} = dN/dt$ is the nucleation rate and G is the crystal growth rate, which was obtained from Azzurri (2003). The nucleation rate can be divided into a contribution from flow and from temperature changes, $\dot{N} = (dN_{nf}/dt) + (dN/dt)\dot{T}$. In all results presented in this study, $\dot{T} = 0$. The total number of nuclei is the sum of the quiescent nucleation density and the flow-induced nuclei obtained from the nucleation model described above, $N = N_q + N_{nf}$. In the short-term shear experiments presented in this study, N_q is negligible as it is much smaller than N_{nf}. For continuous flow experiments, N_q was obtained from the experiments with the lowest flow rate, where the flow is assumed to have no influence on the nucleation density. V_{tot}, S_{tot}, and R_{tot} denote per unit volume the total volume of spherulites, their total surface, and the sum of their radii, respectively. The Kolmogorov-Avrami model was used to correct for impingement [Avrami (1939, 1940)]

$$1 - \xi = \exp(-\phi_0), \tag{8}$$

where ϕ_0 is the undisturbed volume of spherulites and ξ is the volume fraction (or space filling) after correcting for impingement. The space filling of spherulites is used as input in the suspension model used by Steenbakkers and Peters (2008) and Roozemond *et al.* (2012), which predicts from crystalline volume fraction the relative dynamic modulus $f_G^* = G^*/G_0^*$, with G_0^* the dynamic modulus of the melt. Further information is given in Appendix B.

The viscosity for the longest mode is calculated using the Rolie-Poly model, taking into account relaxation time increase due to flow-induced nuclei. For the other modes, we used linear viscoelastic Maxwell-like behavior to calculate the dynamic viscosity. From the dynamic viscosity, assuming the Cox-Merz rule holds [Cox and Merz (1958)], we obtained the shear viscosity. The sum of all modes is multiplied with the relative modulus from the suspension model. For shear, this becomes

$$\eta(t) = |f_G^*| \frac{G_M B_{e12}(t)}{\dot{\gamma}} + \left| f_G^* \left(\sum_{k=1}^{M-1} G_k \left(\frac{\dot{\gamma}\lambda_k^2}{1 + \lambda_k^2 \dot{\gamma}^2} + i \frac{\lambda_k}{1 + \lambda_k^2 \dot{\gamma}^2} \right) \right) \right|, \tag{9}$$

with G_k and λ_k the shear modulus and reptation time of mode k respectively, M the number of Maxwell modes, and B_{e12} the 12 component of the elastic Finger tensor from the Rolie-Poly model. For extensional flow, we have

$$\eta_E^+(t) = |f_G^*| \frac{G_M (B_{e11}(t) - B_{e22}(t))}{\dot{\varepsilon}} + |f_G^*| \sum_{k=1}^{M-1} 3 G_k \lambda_k \left(1 - \exp\left(-\frac{\lambda_k}{t} \right) \right), \tag{10}$$

where B_{e11} and B_{e22} are the 11 and 22 components of the elastic Finger tensor.

V. RESULTS

First, parameter sets for PB800 and BR200 are determined by fitting results from our model to data from short-term shear experiments which give nucleation density for various shear rates, shear times, and temperatures. Next, calculations for continuous flow experiments are presented and compared to experimental data. For grades PB800 and BR200, the same parameter sets as for the short-term shear experiments are used. For PB400, parameters are determined by fitting to the continuous flow experiments.

A. Short-term shear flow experiments

Figures 3 and 4 show the nucleation density of PB800 and BR200 after short-term shear at different temperatures. The horizontal axis shows the duration of shear; symbols indicate shear rate. The vertical axis indicates the nucleation density observed during isothermal crystallization after cessation of flow. PB800 was held at the shear temperature to crystallize, BR200 was cooled down to 92 °C and crystallization was monitored at that temperature. An Arrhenius-like temperature dependence of g_n was implemented

$$g_n(T) = g_{n,\mathrm{ref}} \exp\left(\frac{E_{a,g}}{R}\left(\frac{1}{T} - \frac{1}{T_{\mathrm{ref}}}\right)\right). \tag{11}$$

Here, T is the temperature at which flow is applied. Three parameters are now required per material to calculate nucleation density for all experiments: $g_{n,\mathrm{ref}}$, the parameter coupling backbone stretch to nucleation rate at a reference temperature, $E_{a,g}$, governing the temperature dependence of g_n, and α, governing the relaxation time increase due to the physical cross-links generated by the flow-induced nuclei. The reference temperature in Eq. (11) was taken to be 100 °C in all cases. The three parameters (see Table IV) were determined by least squares fitting to the short-term shear experiments for PB800 and BR200. Although BR200 appears to be vastly more susceptible to flow-enhanced nucleation (compare 10 s^{-1} at 94 °C for PB800 and 0.7 s^{-1} at 100 °C for BR200), the parameter values are remarkably close to those of PB800, suggesting that their chemistry is similar and the major difference is their chain length and hence relaxation times. Zuidema *et al.* (2001) proposed scaling the parameter coupling nucleation rate to molecular stretch g_n with the rheological shift factor a_T, which was validated by Steenbakkers (2009). In contrast, we find no relation between $g_n(T)$ and a_T. PB800, which has a lower flow activation energy than BR200, shows that g_n depends much more strongly on temperature. In both cases, the activation energy governing the temperature dependence is higher than for a_T,

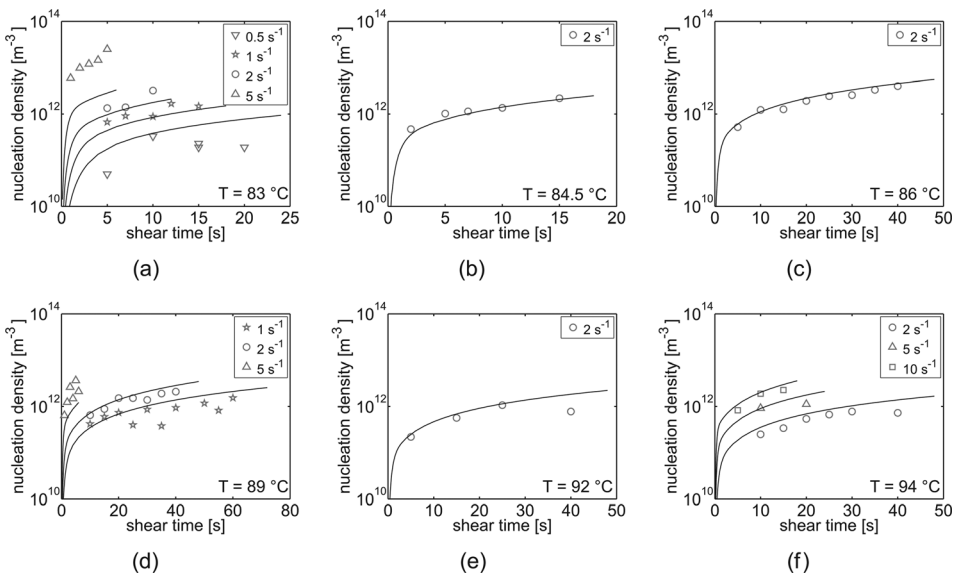

FIG. 3. Nucleation density versus shear time after short-term shear flow of PB800. Different subfigures are different shear and crystallization temperatures. Symbols indicate experimental data, and solid lines are calculations with the parameters in Tables II and IV.

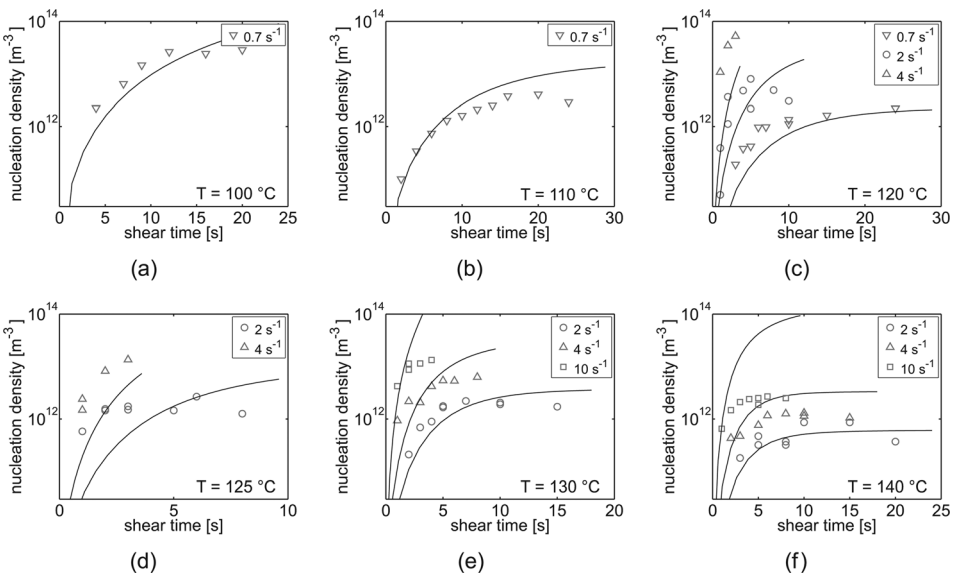

FIG. 4. Nucleation density versus shear time after short-term shear flow of BR200. Different subfigures are different shear temperatures. The crystallization temperature is 92 °C in all cases. Symbols indicate experimental data, and solid lines are calculations with the parameters in Tables II and IV.

in the case of BR200 only slightly but for PB800 a factor 2.5. However, in the narrower temperature range investigated by Steenbakkers *et al.*, $g_n \sim a_T$ might be a sufficiently good approximation. The parameter α governing relaxation time increase caused by flow-induced nucleation sites is the same order of magnitude for both materials.

The calculations and experimental data show good agreement. For the majority of shear rates and temperatures, the model is able to capture the experimental data quantitatively. At higher shear rates, however, the calculations deviate from the experimental results. Especially the experiments with higher shear rates for PB800 [Figs. 3(a) and 3(d)] show a much higher nucleation rate. The performance of the model might improve by incorporating the distinction between precursors and nuclei, as discussed in Sec. III. However, the main aim of this work is to validate the modeling framework for continuous flow experiments, which are all in the low shear rate regime. Therefore, we expect this formulation of our nucleation model to be satisfactory for current purposes. For modifications to the current model that would make it more suitable to the high-shear rate regime, the reader is referred to Steenbakkers and Peters (2011).

1. Apparent saturation of nucleation density

A striking qualitative difference between the two materials is the nonlinearity of nucleation density versus shear time. For PB800, the nucleation density can reasonably

TABLE IV. Parameters in the nucleation model determined by fitting to short-term shear experiments (PB800, BR200) or continuous shear flow experiments (PB400).

	PB800	PB400	BR200
$g_{n,\mathrm{ref}}$ (m^{-3} s^{-1})	4.9×10^{10}	2.5×10^{9}	4.1×10^{10}
$E_{a,g}$ (kJ/mol)	110	100	68
α (m^3)	6.3×10^{-14}	2.1×10^{-11}	1.0×10^{-14}

accurately be described as linear in shear time, but for BR200, the nucleation density clearly exhibits a high slope for short shear times, which levels off at longer shear times. This phenomenon could be interpreted as saturation, which has been observed in a number of studies [Baert *et al.* (2006); Housmans *et al.* (2009); Kumaraswamy *et al.* (1999); Vleeshouwers and Meijer (1996)]. Some authors have hypothesized saturation to be caused by depletion of polymer chains above a certain critical molecular weight [Baert *et al.* (2006); Somani *et al.* (2000); Steenbakkers (2009)]. However, in the current experiments, the saturation-like behavior can be explained purely from a rheological considerations. Figure 5 shows for both materials the stretch of the hmw tail and the resulting nucleation rate for different shear rates at one temperature. As the longest Rouse time for BR200 is much higher than for PB800 (see Table III), it takes much longer for the stretch to reach a steady state. Therefore, the overshoot in chain stretch is much larger for BR200 than for PB800. During this overshoot, the nucleation rate is higher, as it is directly coupled to chain stretch. Only when the chain stretch reaches steady state, the nucleation rate reaches a constant value. Consequently, the flow-induced nucleation density of PB800 continuously increases (as there is hardly an overshoot in chain stretch), and the data for BR200 distinctly level off (because the nucleation rate is much higher during the overshoot than in steady state). This could be (mistakenly) interpreted as some kind of saturation.

B. Continuous flow experiments

1. Continuous shear flow

We validate our modeling framework for continuous flow with continuous shear flow experiments on PB800 performed by Acierno *et al.* (2008), using the parameter set that

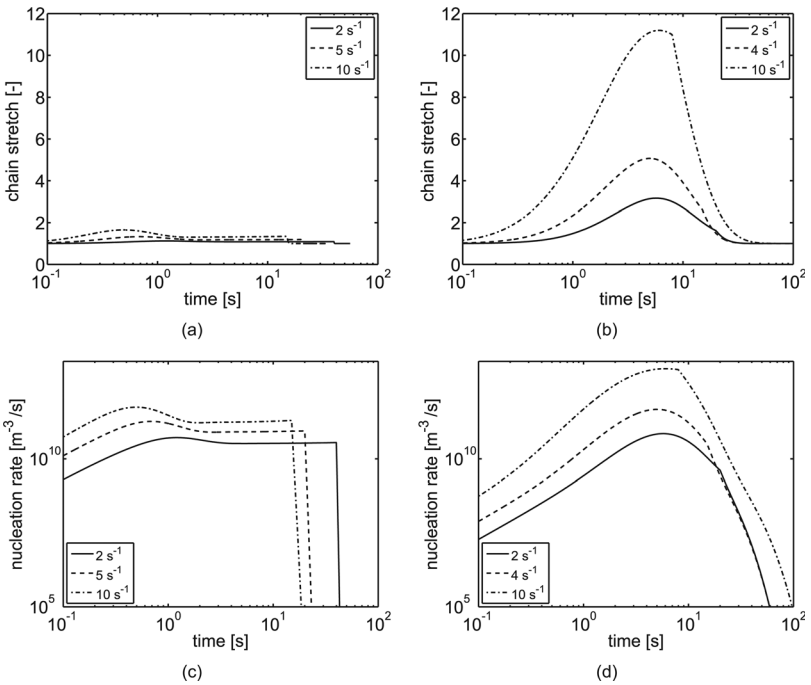

FIG. 5. Stretch of longest mode [(a) and (b)] and resulting nucleation rate [(c) and (d)] in time. (a) and (c) Grade PB800, $T = 94\,^{\circ}\mathrm{C}$, shear rates are 2, 5, and $10\,\mathrm{s}^{-1}$ and shear times 40, 20, and 15 s, respectively. (b) and (d) Grade BR200, $T = 140\,^{\circ}\mathrm{C}$, shear rates are 2, 4, and $10\,\mathrm{s}^{-1}$ and shear times 20, 15, and 8 s, respectively. Note that the slight slope in stretch after the overshoot is caused by the relaxation time increase caused by flow-induced physical cross-links [Eq. (6)].

was determined from short-term shear flow (see Table IV). The quiescent nucleation density was fit to the experiment with the lowest shear rate. Calculations and experiments are compared in Fig. 6. The model performs well over a range of shear rates of nearly three decades, especially considering the fact that the parameter set was fit to experiments done in a different group with a different experimental technique.

Hadinata *et al*. (2005) performed similar experiments on grade PB400, a grade with a molecular weight between PB800 and BR200. Table IV gives the three parameters in the nucleation model for this material, which were fit to these continuous flow experiments. Calculations and experiments are compared in Fig. 7. Calculations capture the experimental data very well over a range in shear rate of over three decades. The values of the parameters in the nucleation model for PB400 qualitatively differ from those of PB800 and BR200; chain stretch initially causes a lower nucleation rate, but the flow-induced nuclei have a stronger effect on increasing relaxation times. The temperature dependence of g_n roughly follows a_T^2.

2. Contributions to the viscosity increase

The present model accounts for two effects that can increase the viscosity of the material. First, the volume fraction of spherulites, which have a higher stiffness than the surrounding melt, gradually increases. Second, the relaxation time of the hmw tail increases due to flow-induced nuclei acting as physical cross-links. The latter was implemented on empirical basis, as explained in Sec. III. If this mechanism proves necessary to predict the experimentally observed viscosity, the present results could indirectly provide evidence for such a mechanism.

The contributions from both effects (relaxation time increase and suspension behavior) for continuous flow of PB400 at 107 °C are presented in Fig. 8. We observe that the viscosity increase in the calculations is dominated by suspension-like behavior; the contribution from relaxation time increase is too weak to be noticeable for these flow conditions. Hence, these results do not provide evidence that flow-induced nuclei increase relaxation times.

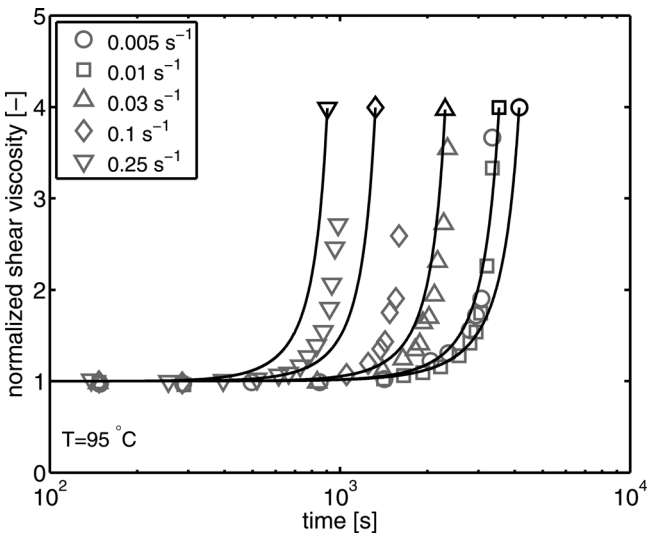

FIG. 6. Time evolution of normalized shear viscosity in PB800 for a range of shear rates at 95 °C. Symbols show measurements; solid lines show calculations with parameters as in Tables II and IV.

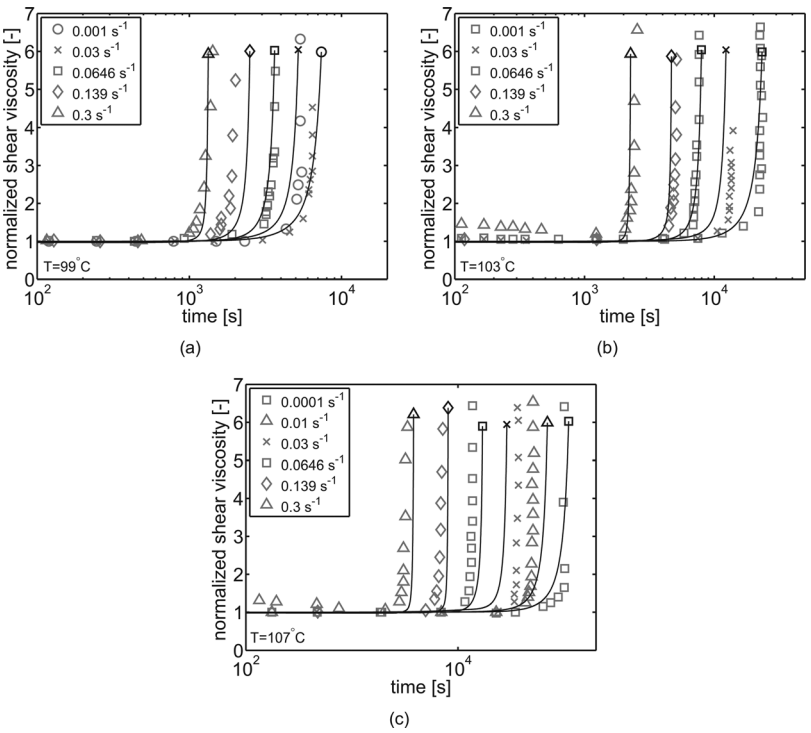

FIG. 7. Time evolution of normalized shear viscosity in PB400 for a range of shear rates. Different subfigures are different temperatures. Symbols show measurements; solid lines show calculations with parameters as in Tables II and IV.

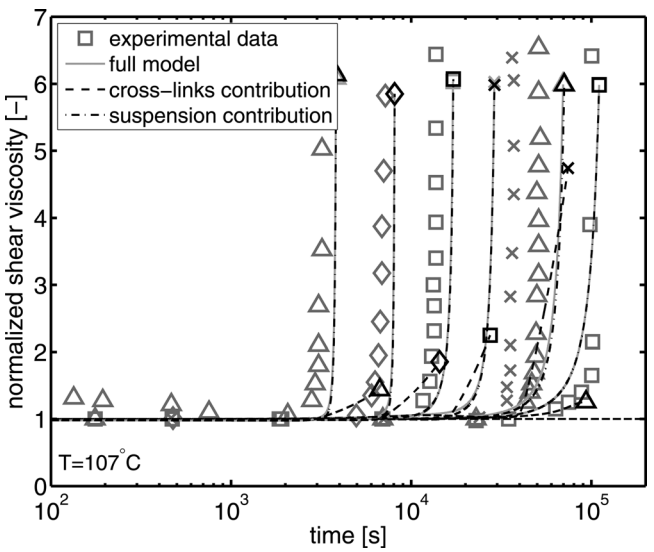

FIG. 8. Time evolution of normalized shear viscosity in PB400 for a range of shear rates at 107 °C. Symbols show measurements. Solid lines shows calculations with the full modeling framework, dashed-dotted lines show contribution from the suspension model, dashed lines show contributions from relaxation time increase due to physical cross-links from flow-induced nuclei.

3. Continuous extensional flow

Using an EVF fitted to a conventional rheometer, Hadinata *et al.* (2007) performed continuous uniaxial extensional flow experiments on grade BR200. The morphology created in these experiments is presumably highly oriented, for extensional rates with Weissenberg numbers based on stretch greater than unity for the longest chains, $\mathrm{Wi}_R = \dot{\epsilon}\lambda_R^{-1} > 1$ [van Meerveld *et al.* (2004)]. Table III shows values of the longest Rouse time. The measurements in this regime are indicated in open symbols in Fig. 9. If the crystalline structure becomes highly oriented, the current model does not apply, as it describes only crystallites that grow in three dimensions and form a suspension of spherical particles. Therefore, the results of the present model in these conditions should be regarded with care.

Experiments and calculations show excellent agreement for all extension rates (see Fig. 9). The model should indeed apply for $\mathrm{Wi}_R < 1$, but surprisingly, the calculations also capture the experiments exceptionally well in the range of strain rates, where $\mathrm{Wi}_R > 1$ and where Hadinata *et al.* (2007) observed "strain-induced crystallization" (i.e., the viscosity upturn occurring at the same Hencky strain, independent of strain rate). This remarkable result deserves further explanation. Investigation of the contributions of the simulated viscosity shows that the viscosity upturn at these strain rates is actually not caused by crystallization (see Fig. 10). Instead, the viscosity of the longest mode, calculated with the Rolie-Poly model, grows unboundedly because $\mathrm{Wi}_R > 1$ and hence the long chains are in the stretching regime.

The viscosity upturn observed in experiments is not caused purely by this strain hardening, because the long chains are finitely extensible which is not included in the Rolie-Poly model; at temperatures above the melting temperature, a slight strain hardening can be expected [Hadinata *et al.* (2007)], but not nearly the viscosity upturn as observed here. Hence, the current model replicates the experimental results without taking into account the complete physical picture. Including all relevant physics would require a description of the nucleation and growth of oriented structures and a suspension model for cylindrical structures, which is outside the scope of this work. Nonetheless, the current model may give some insight into the mechanism of strain-induced crystallization. We hypothesize that strain hardening due to stretch- and strain-controlled crystallization is strongly related: At the strain that chains enter the stretching regime, they act as extremely efficient nucleation sites, causing nearly instantaneous crystallization.

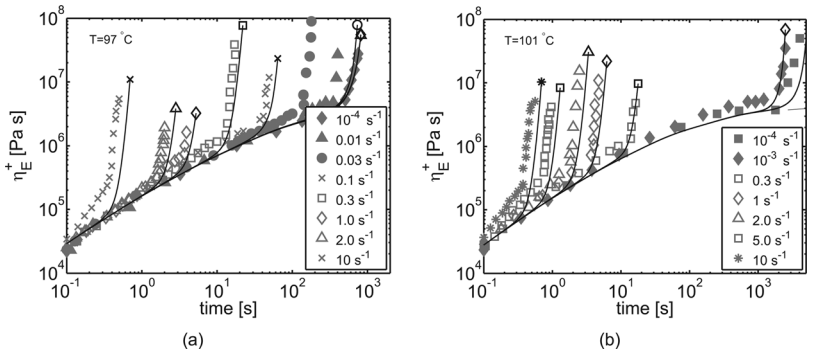

FIG. 9. Time evolution of transient extensional viscosity in BR200 for a range of extension rates. Different subfigures are different temperatures. Symbols show measurements; solid lines show calculations with parameters as in Tables II and IV. Closed symbols show measurements with $\mathrm{Wi}_R < 1$, open symbols are measurements with $\mathrm{Wi}_R > 1$.

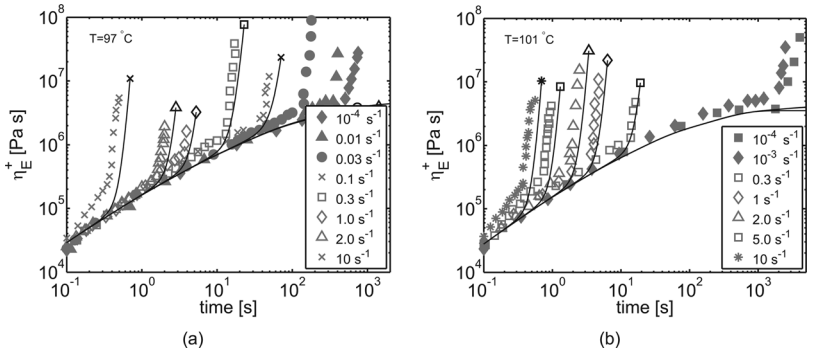

FIG. 10. Time evolution of transient extensional viscosity in BR200 for a range of extension rates. Different subfigures are different temperatures. Symbols show measurements; solid lines show the calculated viscosity, purely from linear viscoelastic behavior for all modes but the slowest, and calculation with the Rolie-Poly model for the slowest mode. Nucleation is turned off. Closed symbols show measurements with $\mathrm{Wi}_R < 1$, open symbols are measurements with $\mathrm{Wi}_R > 1$.

We should note that Hadinata *et al.* (2007) did study strain hardening and found no relation with the sharp viscosity upturn. However, they calculated strain hardening caused by entanglements acting as long chain branches using the molecular stress function (MSF) model [Wagner *et al.* (2001)]. This model does not explicitly calculate chain stretch, which might be the reason that they did capture the initial deviation from the linear viscoelastic envelope but did not see the sharp upturn coinciding with crystallization.

Both Derakhshandeh and Hatzikiriakos (2012) and White *et al.* (2012) also observed the viscosity upturn at constant strain in extensional flow. Derakhshandeh and Hatzikiriakos (2012) performed experiments on two grades of high-density polyethylene of which Ansari *et al.* (2010) studied the rheology. As the onset of the terminal regime is not shown, we are not able to estimate the longest relaxation times. But as both these materials have a high-polydispersity index, it is likely that the strain rates in their experiments are in the stretching regime for the long chains.

White *et al.* (2012) observed strain-induced crystallization in extensional flow of iPP. Figure 2 in their paper shows that the longest reptation time is in the order of 100 s for the material they used, which, following Eq. (1), gives an estimate for the longest Rouse time of $\sim$1 s. They observed strain-induced crystallization for $0.01\,\mathrm{s}^{-1} < \dot{\epsilon} < 0.1\mathrm{s}^{-1}$. This is not in the stretching regime for this estimate of the longest Rouse time, and hence, this would contradict that strain-induced crystallization is related to chain stretch. However, in previous work we have shown that for similar materials, this method of estimating the longest Rouse time is inaccurate [Roozemond *et al.* (2011); Steenbakkers and Peters (2011)].

VI. CONCLUSIONS

A modeling framework was presented to calculate flow-induced nucleation density and the evolution of viscosity under the influence of nucleation-enhancing flow. The model couples nucleation rate to molecular deformation, which is calculated from flow conditions via rheological characteristics, i.e., relaxation times. This intermediate step of calculating molecular deformation from a rheological constitutive model has proven to be vital in understanding flow-induced crystallization experiments.

We have shown that the model provides predictive capabilities in shear as well as extensional flow. Good agreement was obtained with short-term shear experiments on

poly(1-butene). By combining the nucleation model with a suspension model, introducing no additional parameters, excellent agreement with the viscosity signal in continuous flow experiments was obtained.

The model provides a tool for interpreting some experimental observations. First, the saturation-like effect in flow-induced number density, at least in the present experiments, can be explained solely from the stress overshoot after flow startup. Because the polymer chains experience large deformations during this overshoot, the nucleation rate also shows an overshoot before reaching steady state, thus causing a saturation-like effect in flow-enhanced nucleation density. This phenomenon was predicted to be more pronounced in materials with higher relaxation times, which is confirmed by experiments. The saturation level, i.e., the value at which nucleation density seemingly reaches a plateau, is highly dependent on shear rate. Second, we believe the upturn in extensional viscosity, occurring at constant strain during continuous flow, to be caused by chains in the hmw tail entering the chain stretch regime, causing nearly instantaneous crystallization.

ACKNOWLEDGMENTS

The authors would like to thank Professor G. C. Alfonso for kindly sharing the data for the short-term shear experiments. This work is part of a collaboration with the group of Professor Julia Kornfield at the California Institute of Technology. The project is supported by the Dutch Technology Foundation (STW), Grant No. 08083, and the National Science Foundation (NSF), Grant No. DMR-0710662.

APPENDIX A: SIMPLIFICATIONS WITH RESPECT TO THE FULL MODEL

In this appendix, the full nucleation model that was used by Steenbakkers and Peters (2011) is briefly reiterated, after which we highlight the omissions that result in the simplified version of the model that was used in this paper.

In the full model, as used by Steenbakkers and Peters (2011), the deformation of chains spawns flow-induced precursors, which transform into nuclei with a typical timescale τ_{pn}

$$\frac{dN_{pf}}{dt} = g_n\left(\Lambda^4_{\mathrm{hmw}}(t) - 1\right) - \frac{N_{pf}}{\tau_{pn}}, \tag{A1}$$

$$\frac{dN_{nf}}{dt} = \frac{N_{pf}}{\tau_{pn}}. \tag{A2}$$

Here, N_{pf} is the number density of flow-induced precursors and N_{nf} is the flow-induced number density of nuclei. The distinction between precursors and nuclei is a necessary one, as Steenbakkers and Peters (2011) discussed, because flow (if sufficiently strong) interferes with nucleation. For this reason, all flow-induced nuclei after short-term flow have the same radius at any point in time, within the resolution of an optical microscope [Hristova *et al.* (2004); Stadlbauer *et al.* (2004)]. Also in film drawing, it was observed that flow impedes nucleation [Blundell *et al.* (1996, 2000); Mahendrasingam *et al.* (1999)]. For this reason, Steenbakkers and Peters (2011) took the time scale for nucleation τ_{pn} to be infinite during flow and zero after cessation of flow, i.e., no nucleation during flow and instant nucleation after flow. For continuous flow experiments, where nucleation does in fact occur during flow, because the flow rates are too low to interfere with nucleation, this would have to be modified to, for example,

$$\tau_{pn} = \tau_{pn,Q} \exp(\zeta(\Lambda_{\text{hmw}} - 1)), \tag{A3}$$

where $\tau_{pn,Q}$ is the nucleation time in quiescent conditions, which is expected to be much smaller than the typical time for crystallization. The parameter ζ determines how strongly τ_{pn} increases with flow. For the limit of no or very strong flow, this expression results in what was implemented by Steenbakkers and Peters (2011), i.e., $\tau_{pn} = \tau_{pn,Q} \approx 0$ in quiescent conditions and $\tau_{pn} \approx \infty$ during strong flows.

Further, Steenbakkers and Peters (2011) postulated that only precursors, not nuclei, act as physical cross-links. The relaxation time increase in that case is given by

$$\frac{\lambda_{j,\text{hmw}}}{\lambda_{j,\text{hmw},0}} = (1 + \alpha N_{pf}). \tag{A4}$$

Thus, the effect on the rheology disappears as soon as the precursors nucleate. This argument was introduced for practical reasons: At some point, the influence on the relaxation times of the precursors has to relax, otherwise, when the flow is stopped, the relaxation of chain stretch might be balanced out by the relaxation time increase due to creation of precursors. Consequently, the number of flow-induced nuclei would keep growing to infinity. For a more detailed argumentation, the reader is referred to Steenbakkers and Peters (2011).

1. Simplifications

We choose to omit the intermediate step of nucleation precursors, for the reason that including this step requires two additional parameters [ζ and $\tau_{pn,Q}$ in Eq. (A3)], whilst it does not significantly change the final nucleation density. Moreover, because the shear rates considered in this work are relatively weak, we can get away with assuming that nucleation sites do retain their effect on the relaxation times after nucleation; because the relaxation times increase at most by a factor of two in the current experiments ($\alpha \approx 10^{-14}$ and $N_{nf} \approx 10^{14}$), we have no problems with the number of flow-induced nuclei growing to infinity.

APPENDIX B: HARDENING BEHAVIOR OF iP1B

To account for the viscosity increase with increasing crystalline volume fraction, we use the approach of Roozemond *et al.* (2012) and Steenbakkers and Peters (2008). The material is considered as a suspension of spheres (spherulites) in a viscoelastic matrix (the melt). The generalized self-consistent method (GSCM) for spherical particles is used to calculate the viscosity as a function of volume fraction [Christensen (1990); Christensen and Lo (1979, 1986)]. The inputs in this model are the dynamic moduli of the melt and of the spherulites. The latter is taken equal to the dynamic modulus of the fully crystallized material. With these parameters known, we can use the GSCM to predict the shear modulus relative to the modulus of the melt at all intermediate crystalline volume fractions

$$f_G^*(\xi, \omega) = \frac{G^*(\xi, \omega)}{G(\xi = 0, \omega)}, \tag{B1}$$

where f_G^* is the relative dynamic modulus, ξ denotes the volume fraction of crystallites, ω is the oscillatory frequency. The reader is referred to Roozemond *et al.* (2012) for more information on applying the GSCM to crystallizing melts.

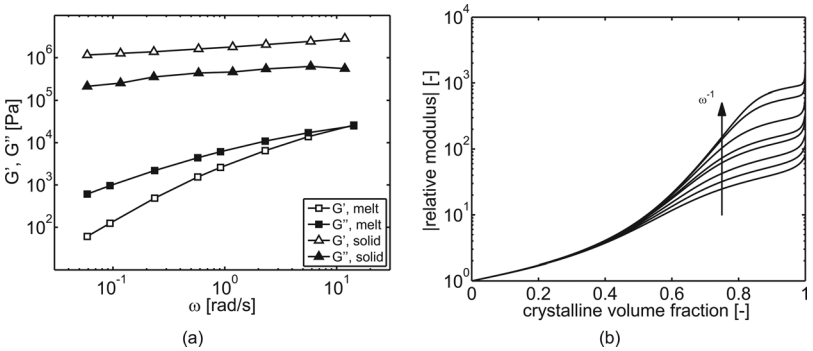

FIG. 11. (a) Frequency sweep of an iP1B at 109 °C. Squares show pure melt, triangles show crystallized material. (b) Absolute value of dynamic modulus normalized with dynamic modulus of the melt versus relative crystallinity for this iP1B from the 3D GSCM.

Coppola *et al*. (2006) measured the storage and loss modulus of the melt and crystallized material at 109 °C for an iP1B with a molecular weight comparable to that of PB400. The data are reproduced in Fig. 11(a). We use these values as input for the suspension model. The prediction of the absolute value of the dynamic modulus relative to the dynamic modulus of the melt at intermediate crystalline volume fractions for all oscillatory frequencies is shown in Fig. 11(b).

The exact values of the ratio between the dynamic modulus of the melt and crystallized material will differ between materials, and hence so will $f_G^*(\xi, \omega)$. However, at low crystalline volume fractions, the suspension model is not very sensitive to changes herein. Because we are only interested in the viscosity increase at low crystalline volume fractions, we expect the GSCM with these parameters to be a sufficiently good approximation. To validate this approach, we apply the GSCM with parameters obtained from Coppola's data to experimental data presented by Bove and Nobile (2002), who measured the storage modulus of crystallizing PB400. We compare their data with a

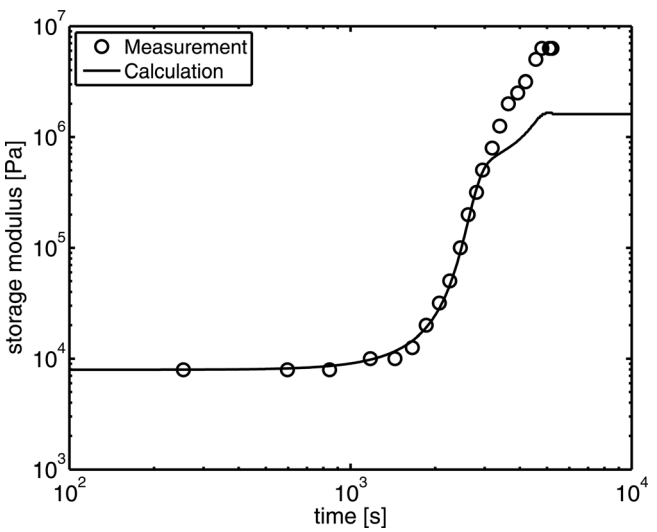

FIG. 12. Time evolution of storage modulus of PB400 crystallizing under quiescent conditions at 95 °C. Symbols show measurements from Bove and Nobile (2002); the line shows prediction of the GSCM with crystalline volume fraction from heterogeneous nucleation and spherical growth.

calculation of the storage modulus with the GSCM, following heterogeneous spherulitical crystallization [Eder and Janeschitz-Kriegl (1997)] for which crystalline volume fraction is given by

$$\xi(t) = 1 - \exp(kt^3), \tag{B2}$$

where ξ is the crystalline volume fraction, t is time, and k is a rate constant which was fit to the data from Bove and Nobile (2002). The measurement was performed at 95 °C at an oscillatory frequency of 1 rad/s, corresponding to a frequency of approximately 0.57 rad/s at 109 °C in the data from Coppola *et al.* (2006). The result is presented in Fig. 12. Indeed, we capture the data quite well at early stages of crystallization, despite the final modulus being underpredicted by nearly an order of magnitude. Therefore, we expect this approach to give a good indication of when the viscosity shows an upturn due to crystallization, even though we do not have exact values for the moduli of the melt and crystallized material.

References

Acierno, S., S. Coppola, and N. Grizzuti, "Effects of molecular weight distribution on the flow-enhanced crystallization of poly(1-butene)," J. Rheol. **52**(2), 551–566 (2008).

Ansari, M., S. Hatzikiriakos, A. Sukhadia, and D. Rohlfing, "Rheology of Ziegler-Natta and metallocene high-density polyethylenes: Braod molecular weight distribution effects," Rheol. Acta **50**, 17–27 (2011).

Avrami, M., "Kinetics of phase change. I: General theory," J. Chem. Phys. **7**(12), 1103–1112 (1939).

Avrami, M., "Kinetics of phase change. II: Transformation-time relations for random distribution of nuclei," J. Chem. Phys. **8**(2), 212–224 (1940).

Azzurri, F., "Melt crystallization and polymorphic transformation in isotactic poly(1-butene) based materials," Ph.D. thesis, University of Genoa, 2003.

Azzurri, F., and G. Alfonso, "Lifetime of shear-induced crystal nucleation precursors," Macromolecules **38**, 1723–1728 (2005).

Azzurri, F., and G. Alfonso, "Insights into formation and relaxation of shear-induced nucleation precursors in isotactic polystyrene," Macromolecules **41**, 1377–1383 (2008).

Baert, J., "Flow-induced crystallization of poly-1-butene," Ph.D. thesis, Katholieke Universiteit Leuven, 2009.

Baert, J., and P. van Puyvelde, "Effect of molecular and processing parameters on the flow-induced crystallization of poly-1-butene. Part 1: Kinetics and morphology," Polymer **47**, 5871–5879 (2006).

Baert, J., P. van Puyvelde, and F. Langouche, "Flow-induced crystallization of PB-1: From the low shear rate region up to processing rates," Macromolecules **39**, 9215–9222 (2006).

Balzano, L., S. Rastogi, and G. Peters, "Crystallization and precursors during fast short-term shear," Macromolecules **42**, 2088–2092 (2009).

Blundell, D., A. Mahendrasingam, C. Martin, W. Fuller, D. MacKerron, J. Harvie, R. Oldmand, and C. Riekel, "Orientation prior to crystallisation during drawing of poly(ethylene terephthalate)," Polymer **41**, 7793–7802 (2000).

Blundell, D., D. MacKerron, W. Fuller, A. Mahendrasingam, C. Martin, R. Oldman, R. Rule, and C. Riekel, "Characterization of strain-induced crystallization of poly(ethylene terephthalate) at fast draw rates using synchrotron radiation," Polymer **37**(15), 3303–3311 (1996).

Bove, L., and M. R. Nobile, "Shear-induced crystallization of isotactic poly(1-butene)," Macromol. Symp. **185**, 135–147 (2002).

Carrot, C., J. Guillet, and K. Boutahar, "Rheological behavior of a semi-crystalline polymer during isothermal crystallization," Rheol. Acata **32**, 566–574 (1993).

Christensen, R., "A critical evaluation for a class of micro-mechanics models," J. Mech. Phys. Solids **38**, 379–404 (1990).

Christensen, R., and K. Lo, "Solutions for effective shear properties in three phase sphere and cylinder models," J. Mech. Phys. Solids **27**, 315–330 (1979).

Christensen, R., and K. Lo, "Erratum: Solutions for effective shear properties in three phase sphere and cylinder models," J. Mech. Phys. Solids **34**, 639 (1986).

Coppola, S., and N. Grizzuti, "Microrheological modeling of flow-induced crystallization," Macromolecules **34**, 5030–5036 (2001).

Coppola, S., S. Acierno, N. Grizzuti, and D. Vlassopoulos, "Viscoelastic behavior of semicrystalline thermoplastic polymers during the early stages of crystallization," Macromolecules **39**, 1507–1514 (2006).

Cox, W., and E. Merz, "Correlation of dynamic and steady flow viscosities," J. Polym. Sci. **28**(118), 619–622 (1958).

Custodio, F., R. Steenbakkers, P. Anderson, G. Peters, and H. Meijer, "Model development and validation of crystallization behavior in injection molding prototype flows," Macromol. Theory Simul. **18**(9), 469–494 (2009).

Danusso, F., "Macromolecular polymorphism and stereoregular synthetic polymers," Polymer **8**, 281–320 (1967).

Derakhshandeh, M., and S. Hatzikiriakos, "Flow-induced crystallization of high-density polyethylene: The effects of shear and uniaxial extension," Rheol. Acta **51**, 315–327 (2012).

Doi, M., and S. Edwards, *The Theory of Polymer Dynamics* (Clarendon, Oxford, 1986).

Eder, G., and H. Janeschitz-Kriegl, "Structure development during processing: Crystallization," in *Processing of Polymers*, Volume 18 of Materials Science and Technology: A Comprehensive Treatment (Wiley-VCH, Weinheim, 1997), pp. 269–342.

Graham, R., and P. Olmsted, "Coarse-grained simulations of flow-induced nucleation in semicrystalline polymers," Phys. Rev. Lett. **103**(11), 115702 (2009).

Graham, R., and P. Olmsted, "Kinetic Monte-Carlo simulations of flow-induced nucleation in polymer melts," Faraday Discuss. **144**, 71–92 (2010).

Hadinata, C., "Flow-induced crystallization of polybutene-1 and effect of molecular parameters," Ph.D. thesis, RMIT University, Melbourne, Australia, 2007.

Hadinata, C., C. Gabriel, M. Ruellman, and H. Laun, "Comparison of shear-induced crystallization behavior of PB-1 samples with different molecular weight distribution," J. Rheol. **49**(1), 327–349 (2005).

Hadinata, C., D. Boos, C. Gabriel, E. Wassner, M. Ruellmann, N. Kao, and M. Laun, "Elongation-induced crystallization of a high molecular weight isotactic polybutene-1 melt compared to shear-induced crystallization," J. Rheol. **51**(2), 195–215 (2007).

Housmans, J., R. Steenbakkers, P. Roozemond, G. Peters, and H. Meijer, "Saturation of pointlike nuclei and the transition to oriented structures in flow-induced crystallization of isotactic polypropylene," Macromolecules **42**, 5728–5740 (2009).

Hristova, D., G. Peters, and H. Meijer, "Flow induced crystallization: Effect of flow strength and temperature," Proceedings of the 228th ACS National Meeting, Philadelphia, 2004.

Janeschitz-Kriegl, H., and E. Ratajski, "Kinetics of polymer crystallization under processing conditions: Transformation of dormant nuclei by the action of flow," Polymer **46**, 3856–3870 (2005).

Janeschitz-Kriegl, H., E. Ratajski, and M. Stadlbauer, "Flow as an effective promotor of nucleation in polymer melts: A quantitative evaluation," Rheol. Acta **42**, 355–364 (2003).

Kimata, S., T. Sakurai, Y. Nozue, T. Kasahara, N. Yamaguchi, T. Karino, M. Shibayama, and J. Kornfield, "Molecular basis of the shish-kebab morphology in polymer crystallization," Science **316**, 1014–1017 (2007).

Kumaraswamy, G., A. Issaian, and J. Kornfield, "Shear-enhanced crystallization in isotactic polyproylene. 1. Correspondence between in situ rheo-optics and ex situ structure determination," Macromolecules **32**, 7537–7547 (1999).

Liedauer, S., G. Eder, H. Janeschitz-Kriegl, P. Jerschow, W. Geymayer, and E. Ingolic, "On the kinetics of shear-induced crystallization in polypropylene," Int. Polym. Process. **8**(3), 236–244 (1993).

Likhtman, A., and R. Graham, "Simple constitutive equation for linear polymer melts derived from molecular theory: Rolie-Poly equation," J. Non-Newtonian Fluid Mech. **114**, 1–12 (2003).

Ma, Z., L. Balzano, and G. Peters, "Pressure quench of flow-induced crystallization precursors," Macromolecules **45**, 4216–4224 (2012).

Mahendrasingam, A., C. Martin, W. Fuller, D. Blundell, R. Oldman, J. Harvie, D. MacKerron, C. Riekel, and P. Engström, "Effect of draw ratio and temperature on the strain-induced crystallization of poly(ethylene terephthalate) at fast draw rates," Polymer **40**, 5553–5565 (1999).

Meijer, H., and L. Govaert, "Mechanical performance of polymer systems: The relation between structure and properties," Prog. Polym. Sci. **30**, 915–938 (2005).

Mykhaylyk, O., P. Chambom, R. Graham, J. Fairclough, P. Olmsted, and A. Ryan, "The specific work of flow as a criterion for orientation in polymer crystallization," Macromolecules **41**, 1901–1904 (2008).

Ottonello, P., "Flow-induced crystal nucleation in polymeric systems," Master's thesis, Industrial Chemistry, University of Genova, Italy, 2003.

Phan-Thien, N., "A nonlinear network viscoelastic model," J. Rheol. **22**, 259–283 (1978).

Phan-Thien, N., and R. Tanner, "A new constitutive equation derived from network theory," J. Non-Newtonian Fluid Mech. **2**(4), 353–365 (1977).

Roozemond, P., R. Steenbakkers, and G. Peters, "A model for flow-enhanced nucleation based on fibrillar dormant precursors," Macromol. Theory Simul. **20**(2), 93–109 (2011).

Roozemond, P., V. Janssens, P. van Puyvelde, and G. Peters, "Suspension-like hardening behavior of HDPE and time-hardening superposition," Rheol. Acta **51**, 97–109 (2012).

Schneider, W., A. Köppl, and J. Berger, "Non-isothermal crystallization of polymers—System of rate equations," Int. Polym. Process. **3**(4), 151–154 (1988).

Schrauwen, B., L. van Breemen, A. Spoelstra, L. Govaert, G. Peters, and H. Meijer, "Structure, deformation, and failure of flow-oriented semicrystalline polymers," Macromolecules **37**, 8618–8633 (2004b).

Schrauwen, B., R. Janssen, L. Govaert, and H. Meijer, "Intrinsic deformation behavior of semicrystalline polymers," Macromolecules **37**, 6069–6078 (2004a).

Seki, M., D. Thurman, J. Oberhauser, and J. Kornfield, "Shear-mediated crystallization of isotactic polypropylene: The role of long chain-long chain overlap," Macromolecules **35**, 2583–2594 (2002).

Sentmanat, M. L., "Miniature universal testing platform: From extensional melt rheology to solid-state deformation behavior," Rheol. Acta **43**(6), 657–669 (2004).

Somani, R., B. Hsiao, A. Nogales, I. Sics, F. Balta-Calleja, and T. Ezquerra, "Structure development during shear flow-induced crystallization of i-PP: In-situ small-angle x-ray scattering study," Macromolecules **33**, 9385–9394 (2000).

Stadlbauer, M., H. Janeschitz-Kriegl, G. Eder, and E. Ratajski, "New extensional rheometer for creep flow at high tensile stress. Part II. Flow induced nucleation for the crystallization of iPP," J. Rheol. **48**, 631–639 (2004).

Steenbakkers, R., "Precursors and nuclei, the early stages of flow-induced crystallization," Ph.D. thesis, Eindhoven University of Technology, 2009.

Steenbakkers, R., and G. Peters, "Suspension-based rheological modeling of crystallizing polymer melts," Rheol. Acta **47**(5–6), 643–665 (2008).

Steenbakkers, R., and G. Peters, "A stretch-based model for flow-enhanced nucleation of polymer melts," J. Rheol. **55**(2), 401–433 (2011).

van Erp, T., "Structure development and mechanical performance of polypropylene," Ph.D. thesis, Eindhoven University of Technology, 2012.

van Erp, T., C. Reynolds, T. Peijs, J. van Dommelen, and L. Govaert, "Prediction of yield and long-term failure of oriented polypropylene: Kinetics and anisotropy," J. Polym. Sci., Part B: Polym. Phys. **47**, 2026–2035 (2009).

van Meerveld, J., G. Peters, and M. Huetter, "Towards a rheological classification of flow induced crystallization experiments of polymer melts," Rheol. Acta **44**, 119–134 (2004).

Verbeeten, W., G. Peters, and F. Baaijens, "Numerical simulations of the planar contraction flow for a polyethylene melt using the XPP model," J. Non-Newtonian Fluid Mech. **117**, 73–84 (2004).

Vleeshouwers, S., and H. Meijer, "A rheological study of shear induced crystallization," Rheol. Acta **35**, 391–399 (1996).

Wagner, M., P. Rubio, and H. Bastian, "The molecular stress function model for polydisperse polymer melts with dissipative convective constraint release," J. Rheol. **45**, 1387–1412 (2001).

White, E. B., H. Winter, and J. P. Rothstein, "Extensional-flow-induced crystallization of isotactic polypropylene," Rheol. Acta **51**, 303–314 (2012).

Ziabicki, A., and G. Alfonso, "Memory effects in isothermal crystallization. I. Theory," Colloid Polym. Sci. **272**, 1027–1042 (1994).

Ziabicki, A., and G. Alfonso, "A simple model of flow-induced crystallization memory," Macromol. Symp. **185**, 211–231 (2002).

Zuidema, H., G. Peters, and H. Meijer, "Development and validation of a recoverable strain-based model for flow-induced crystallization of polymers," Macromol. Theory Simul. **10**, 447–460 (2001).